American Journal of Sciences and Engineering Research
e-ISSN -2348 – 703X, Volume 4, Issue 4, 2021

Lithostratigraphy and Geochemical Studies of Sandstones Type Uranium Deposit in Triassic Formations from the DASA Graben of the Tim Mersoï Basin (Northern Niger)

Sani Abdoulwahid[1*], Moussa Konaté[2], Peter Wollenberg[3].
[1]*Department of Geology, University of Agadez, Niger, PO: 199.*
[2]*Department of Geology, Abdou Moumouni University, Niamey, Niger, PO: 10662.*
[3]*Global Atomic Corporation Toronto, Canada Global Atomic Corporation Toronto, Canada*

Abstract: *The DASA graben is located within the Tim Mersoï basin, Northern Niger, and is well known for its high grade uranium mineralization in Carboniferous and Jurassic sediments.*

Uranium in Triassic formations have not been mentioned anywhere in the Tim Mersoï basin previously. The main objective of this study is to investigate the geochemistry of sandstone type-uranium deposits of the Triassic for provenance, paleo-redox and tectonic settings in order to propose a uranium genesis model. Methodologies used in this work consist of lithologic description, Inductively Coupled Plasma Emission Spectrometry (ICP-ES) and Inductively Coupled Plasma Mass Spectrometry (ICP-MS) through lithium metaborate. Results of the geochemical analysis indicate that the sandstone-type uranium deposits of the Triassic formations can be classified into Protoquarzite (i.e. lithearenite and sublitharenite), arkose, subarkose, wacke and Fe-sandwith variations in their maturity. The Rare Earth Elements (REE) pattern shows a significant negative Eu. The high SiO_2 content indicated a quartz rich source rock. The CIA, PIA and CIW values respectively range from 18.78% - 69.01%, 14.56% - 80.26% and 19.97% - 84.51% with an average of 55.798%, 60.45% and 67.30%. These values are variable and may be a result of multiple provenances indicating intense weathering conditions and humid climate at the source area. The geochemical data support deposition in an anoxic environment affected by PM and ACM tectonic settings and the sediments are derived from quartozose sedimentary rocks. In the study area, all samples present Th/U values< 3, suggesting very high uranium enrichment. This is also an indication of intense weathering in the source areas and/or sediment recycling. Uranium would have three sources within the study area:

- *Uranium was leached during the weathering of mafic rocks of the Aïr Mountains in the east;*
- *Uranium was remobilized from Carboniferous and Permian sediments;*
- *Uranium was concentrated by fluid flows through the DASA graben faults.*

Keywords: *DASA Graben, Genesis model, Geochemistry, Triassic formation, Uranium mineralization.*

I. INTRODUCTION

The main Niger uranium deposits are all located in the Tim Mersoï basin to the west of the Aïr Mountains, approximately 200 km north of Agadez. The main deposits exploited or in the process of being exploited (Arlit, Akouta, Imouraren, Madaouéla, DASA) are located to the east of the Arlit fault, which constitutes the main metallotect [1] [2] [3] [4].

Received- 16-07-2021, Accepted- 03-08-2021

However, recent studies carried out in the mineralized areas of Arlit (Tamgak, Akola and Akouta sectors for the Arlit/Akouta area and Imca/Imarine for the Imouraren area) have shown interesting uranium showings to the west of the Arlit fault.

Thus, started in 2008, drilling campaigns were undertaken to conduct an in-depth reconnaissance of these zones where high uranium grades were discovered. This led to a re-evaluation of the metallogenic model of uranium mineralization in the basin [4]. In addition, more recent exploration campaigns (DASA sector, Global Atomic Corporation) have revealed very high-grade U mineralization in some Triassic formations. The discovery of these interesting grades (never mentioned in the Tim Mersoi basin previously) has encouraged the continuation of uranium prospecting in the area. The objective of this study is the lithological and geochemical characterization of this Triassic mineralization. This will undoubtedly contribute to a better understanding of the uranium mineralization in the Tim Mersoï basin.

II. GEOLOGICAL SETTING

A. Study area

The study area is located in the Tim Mersoi basin, more precisely between the mining town of Arlit to the North West (NW) and the coal trough of Anou Araren to the South East (SE) (**Fig. 1**). It covers an area of about 30 km^2. It corresponds to a graben zone, limited by normal faults N70° and also showing a flexure fault called Adrar Emoles. At the level of this area we also note other secondary directions no less important which are the direction N120° to N150° and the E-W faults.

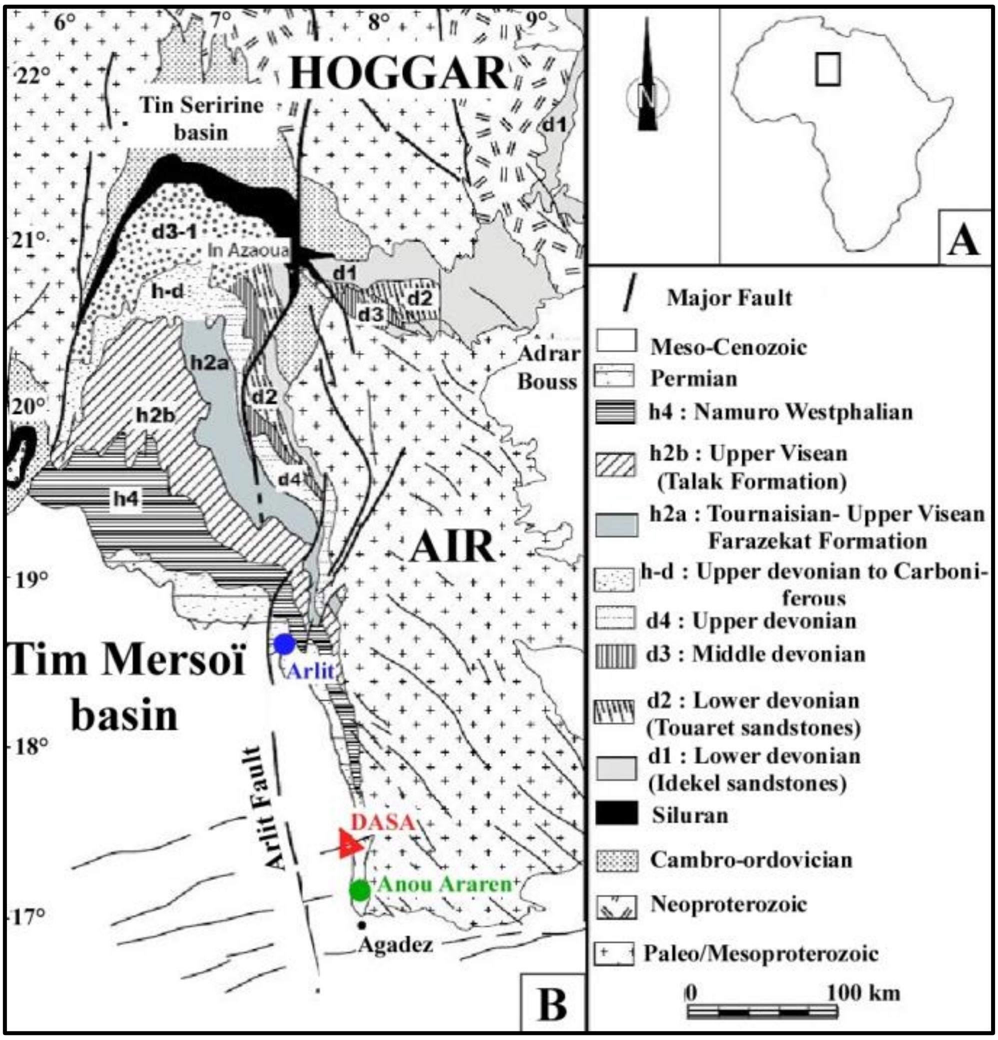

Figure 1: Geological map of the Tim Mersoï basin (modified after [5]). **A :** Position in Africa, **B :** Position of the study area in the Tim Mersoï basin.

B. Geological setting

The Paleo-Mesozoic Tim Mersoi basin (**Fig. 1**), well known for its uranium mineralization, is a sub-basin of the larger Iullemmeden basin (NE Niger) The sediments of this basin were deposited on a metamorphosed basement composed mainly of Cambrian and Precambrian rocks. In the Tim Mersoï basin, the first detrital material was deposited during the Carboniferous and was derived mainly from the Aïr Mountains [6] [7] which are composed of Cambrian and Precambrian gneisses and granites, Devonian plutonic rocks, and volcanic complexes [8] (**Fig. 2**). According to [7], detrital material of this basin, from the Permian to the Cretaceous, was derived from the Aïr Mountains, Zinder area, and Nigeria areas and transported, after erosion, to the north and northwest, and deposited as channel fill sandstones, interbedded with floodplain mudstones [9].

From a lithostratigraphic point of view, the sedimentary rocks overlying the basement are divided into six groups from the Visean to the Lower Cretaceous (**Fig. 2**).

a. The Terada Group (Lower Visean to Upper Visean). It includes various formations (mudstones, sandstones, and siltstones) and is composed of two distinct mega-sequences [6].

- The first one (at the base) is characterized by two fluvial and fluvio-lacustrine episodes (Teragh and Tindirenen formations),
- And the second one (to the top) is characterized by a fluvial and fluvio-glacial episode (Farazekat Formation) and ending with marine deposition of a continental platform (Talak Formation).

b. The Tagora Group (Upper Visean to Namurian-Westphalian). This group is generally subdivided into two mega-sequences that correspond to two similar cycles. These are composed successively of :

- A marine regression, processes of erosion and the formation of fluvial channels, followed by sedimentation in a fluvio-deltaic environment. The lower series contains the conglomerates of the Teleflak Formation and the continental sandstones of the Guézouman Formation, overlain by mudstones and sandstones of the Tchinézogue Formation separated by a discontinuity.
- The upper series is composed of the continental sandstones of the Tarat Formation, the interbedded mudstones-arkoses sequence of the Madaouela Formation, and the eolian sandstones of the Arlit Formation.

c. The Izegouandane Group (Permian) follows with the series of Tagora and marks the appearance of the first detrital terrigenous red series of the Tim Mersoï Basin, which includes intercalated pyroclastic levels originating from the weathering of volcanic rocks. These are fluvial formations deposited in a hot and arid climate. From top to bottom, the group is composed of :

- arkoses with lenses of red clays of the Izegouande Formation,
- mudstones and calcite-cemented brown sandstones of the Téjia Formation,
- siltstones and fine to medium carbonated sandstones of the Tamamaït Formation,
- red mudstones at conglomeratic sandstones rich in analcime [10] [6] of the Moradi Formation.

d. The Agadez Group (Triassic- Jurassic-Lower Cretaceous) overlies the Izegouandane Group, which consists, from base to top, of :

- The Aguelal series, composed of conglomerates and fine-grained sandstones of the Teloua I Formation,
- Succeeded by the Goufat series composed of the arkosic sandstones of the Teloua II Formation and the multicolored sandstones of the Teloua III Formation, rich in analcime.

e. These are overlain by the Wagadi series, composed of the Mousseden unit represented by conglomerate sandstones, the Tchirezrine I arkosic sandstones including intercalation of clay and analcime horizons, and the Abinky Formation composed of massive analcimolite. These are overlain by the Dabla series that begins with arkosic sandstones rich in analcimolite intraclasts of the Tchirezrine II Formation.

f. The Irhazer Group (Lower Cretaceous) includes, at the bottom siltstones of the Assaouas Formation and at the top mudstones of the Irhazer Formation. The Tegama Group (Lower Cretaceous) constitutes the last fluvial sandstone deposits before the Upper Cretaceous marine transgression.

From a structural point of view, four main directions are observed in the Tim Mersoï basin and its cover : N-S, N30°, N70–80° and N140–150° (**Fig. 2**). The N-S lineament of Arlit-In-Azaoua, also known as the Arlit Fault, is the only N-S structure that is expressed in the sedimentary cover, and has a length of more than 100 km. The largest U deposits are located along this major fault. The N30° structures are expressed in the basement and also in the sedimentary cover in the form of flexures. Three large N30° major lineaments (Madaouela-Térada, Zéline-Tesseroukane and Adrar Emoles) along the eastern border of the basin are known. [6] and [11] have demonstrated the role of the N70–80° structures in the sedimentation of the Guézouman sandstones and the Akola unit, particularly during the Visean. The N140–150° structures are much more discreet in the sedimentary cover. The Arlit Fault is associated with many N140–150° structures in the Arlit mining area.
The Tim Mersoï Basin consists of sedimentary series whose formations contain uranium ore deposits that date from the Lower Carboniferous for the Arlit-Akokan, Madaouela and DASA deposits, from Triassic for the DASA deposit and Jurassic to Lower Cretaceous for the Azelik, Imouraren and DASA deposits (**Fig. 2**).

The Arlit-Akonan uranium deposits are hosted by fluvial sandstone of Visean age (Lower Carboniferous; 326–345 Ma – International Commission on Stratigraphy, 2005) alternating with clay layers. The sandstones belong to the Guezouman and Tarat formations. The mineralized layers occur in lenticular bodies at the base of paleo-channels and represent a thickness of about 20 to 25 m, with a uranium concentration of 0.25% UO2 (average deposit content). The channels are structures rich in organic matter, favorable to the trapping of uranium.
Several authors [12] [13] [14] showed the related nature of the mineralization relative to the sedimentary structures (epigenetic concentrations). The works studied type III organic matter from plant fragments which underwent the epigenetic process to pitchblende.

[1] revised the maximum burial of the Guezouman Formation obtained by [15] and dated it as Lower Cenomanian (apatite fission track), in the Tegama Group. These deposits are recorded in the basin during Early and Middle Cretaceous [16]. Maximum burial depth was between 1250 and 2300 m (with a thickness of 200–1050 m for the Lower Cretaceous sediments) (**Fig. 2**). With only the burial effect, 120 Ma are necessary to reach temperatures above 110 °C. This is consistent with the thermal history as defined by fission track data [3].

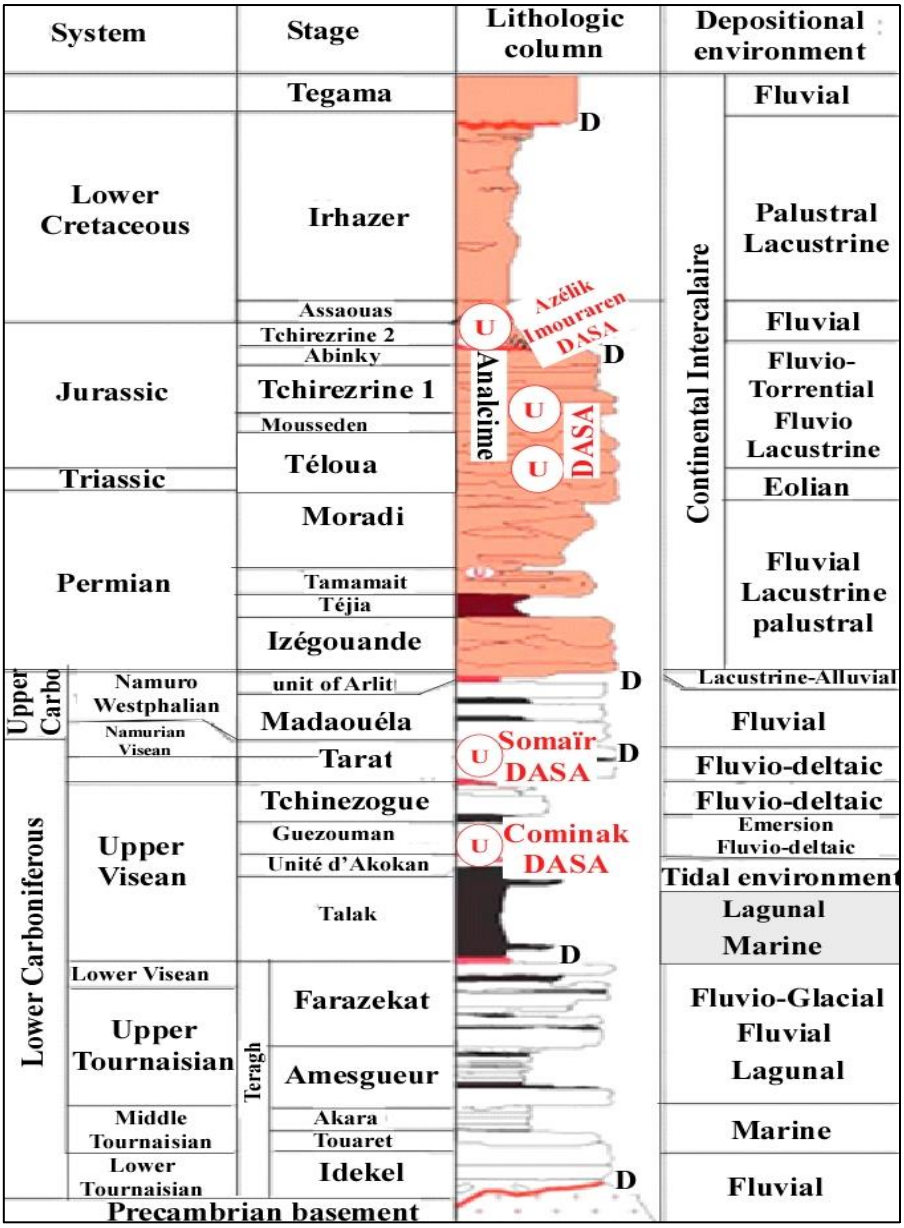

Figure 2: Lithostratigraphic column of the Tim Mersoï basin (After [7] modified).

III. MATERIAL AND METHODS

This study was conducted as follows : the field work included geological studies and the collection of representative samples for laboratory studies. The laboratory analyses included petrographic and geochemical analysis. The petrographic analysis involved thin-sections to help to establish the lithostratigraphy of the Triassic formation for the studied area. Five samples were selected for thin sections which were prepared in the thin section workshop of the Center for Geological and Mining Research (CGMR) in Niger. The samples were analysed by using a petrographic microscope at the laboratory of the Abdou Moumouni University of Niamey, at the Geology department.

Geochemical investigations based on the data of major, trace and rare earth elements (REE) were carried out. A total of **20 samples** were chemically analyzed for their major and trace elements by X-Ray Fluorescence (XRF) in the SGS laboratory in South Africa, and by inductively coupled plasma–atomic emission spectrometry after sample digestion using lithium tetraborate fusion (ICP-AES) in Vancouver Laboratory, Canada while the REE was analyzed by Induced Coupled Plasma-Mass Spectrometry (ICP-MS) carried out in

Vancouver, Canada as well. The concentration of major oxides is usually measured in per cent (%). The trace elements which comprise REE have been measured as parts per million (ppm).

Geochemical data processing including factor and correlation analysis was carried out by using statistical software SPSS-20 and Microsoft excels to determine elemental interrelationship.

IV. RESULTS AND DISCUSSION

C. Lithostratigraphy

The lithostratigraphy has described and organized lithology into distinctive units. The lithology sections are described based on their texture, colour, rock fragments and depth. Five lithofacies have been distinguished (**Fig. 3**).

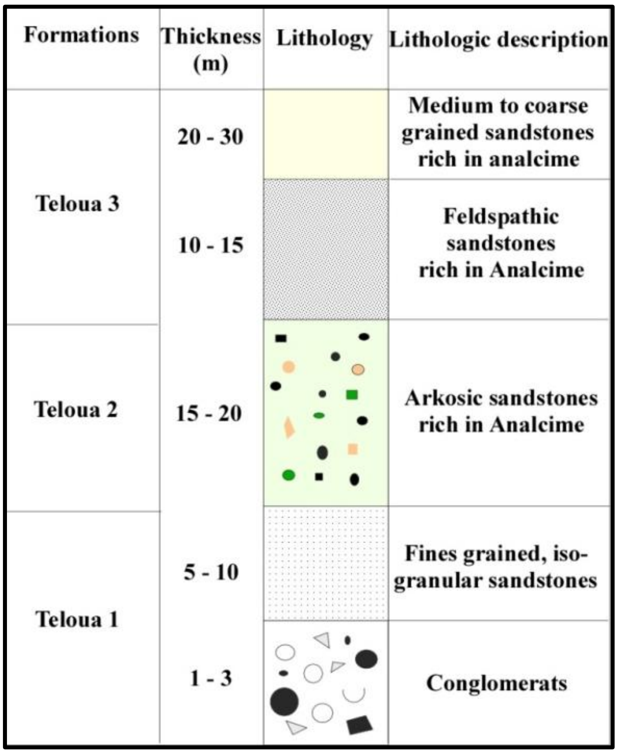

Formations	Thickness (m)	Lithology	Lithologic description
Teloua 3	20 - 30		Medium to coarse grained sandstones rich in analcime
	10 - 15		Feldspathic sandstones rich in Analcime
Teloua 2	15 - 20		Arkosic sandstones rich in Analcime
Teloua 1	5 - 10		Fines grained, iso-granular sandstones
	1 - 3		Conglomerats

Figure 3: Stratigraphy of the Triassic U deposit of the DASA graben.

D. Geochemistry

1) Major Elements Geochemistry

The abundance of the major elements analyzed (**Table 1**) from the study areas shows variation of element composition of all the samples, indicting the heterogeneity of the sediment suite and difference in provenance and sedimentary environment of the sediment. Variations in the chemical deposition reflect changes in the mineralogical composition of the sediments. SiO_2 abundance ranges from 71.481% to 94.023% with an average of 86.086%. This average value is higher than the value of the upper continental crust. This high abundance of SiO_2 from the study areas indicates the dominance of quartz grains in the clastic sediment with little contribution from other detrital source which is also an indication of acidic plutonic igneous rocks. According to the criteria of [17], these average values reflect the quartz-rich nature of the studied sandstones. Also, comparison of the ratio $Al_2O_3/SiO_2 < 1$ and $SiO_2/Al_2O_3 > 1$ respectively confirm the quartz enrichment and high chemical maturity of these studied samples.

Al_2O_3 content of the studied samples is relatively high ranging from 3.480% to 14.984% with an average of 6.301%. The concentration of aluminum can be assigned to the presence of the feldspar and clay mineral in the studied samples.

Fe_2O_3 and TiO_2 which can be assigned to the presence of the alkali and alkaline oxides are very low. The values range respectively from 0.415% to 6.133%, and 0.087% to 0.592%. According to [18] and [19] the low concentrations of Fe_2O_3 and TiO_2 reflect low abundances of Ti-bearing minerals (biotite, ilmenite, titanite and titaniferous magnetite) in the analyzed samples.

The average values of Na_2O and K_2O respectively of 1.539% and 1.608% can be assigned of the presence of Na- and K-feldspars in the studied samples.

MgO, MnO, and P_2O_5 are generally very low averaging 0.480%, 0.092% and 0.062% respectively. The increasing of loss in ignition is related to the presence of kaolinite and mica. The low values of P_2O_5 (averaging 0.062%) and CaO contents (averaging 2.043%) indicates low content apatite in the studied samples.

2) Trace Elements Geochemistry

Geochemistry Trace Elements are very useful especially for the purpose of provenance studies and in deducing provenance setting of sedimentary succession [20] [21] [22] [23]. The trace element concentration of the study area are enriched in Zr and Ba, they are moderately enriched in Cr, Sr, V, and Rb (**Table 2**). Also, trace elemental compositions (**Table 2**) analysis shows variation in their concentration.

However, Ba, U, Cr, Sr, Cu, V, Zr, Y and As present high values while Ga, Hf, Mo, Nb, Ni, Sc, Li, Rb, Th and Ag, Cs, Sn, Tl, Co, Ta, present respectively moderate and low values. According to W, except the six last samples, all others present very lower values.

In addition, the classification scheme for representing trace elements abundance and distribution related to the Upper Continental Crust (UCC) includes the large ion lithophile elements (LILE), Sr and the transition trace element (TTE) Cr, Ni and SC.

A negative correlation of LILE is observed of Sr and Ba with Al_2O_3 (**Fig. 4**). This suggests that their distribution is not mainly controlled by phyllosilicate [24].

The transition trace elements show positive correlation of Ni with Al_2O_3 while Sc with Al_2O_3 show negative one (**Fig. 5**). This suggests that Ni distribution is controlled by phyllosilicate while Sc is not.

Table 1: Major Elemental Compositions.

SiO2	Al2O3	CaO	Fe2O3	K2O	MgO	MnO	Na2O	P2O5	TiO2
91,414	4,440	0,140	1,015	1,638	0,249	0,016	0,674	0,021	0,168
88,903	5,895	0,070	1,058	2,253	0,282	0,013	1,321	0,018	0,087
94,023	2,759	0,574	0,600	1,277	0,116	0,020	0,485	0,011	0,085
81,132	10,260	1,315	2,044	3,301	0,713	0,074	0,647	0,057	0,457
90,274	5,007	0,504	0,543	2,289	0,099	0,055	0,957	0,041	0,155
91,089	4,743	0,294	0,529	2,132	0,116	0,038	0,863	0,041	0,130
84,086	7,936	0,350	2,888	2,843	0,779	0,062	0,903	0,023	0,130
83,274	8,087	1,371	2,302	2,819	0,680	0,082	1,186	0,039	0,160
90,593	4,610	0,434	1,373	1,915	0,332	0,027	0,607	0,023	0,087
85,364	8,182	0,266	1,215	0,385	0,249	0,019	3,774	0,044	0,502
89,663	5,650	0,308	1,187	0,470	0,298	0,050	2,022	0,021	0,332
90,145	5,215	0,266	1,330	0,289	0,298	0,046	2,130	0,023	0,259
71,481	14,133	0,210	6,133	0,554	1,078	0,086	5,581	0,151	0,592
72,781	14,984	0,252	2,616	3,554	0,647	0,058	4,502	0,057	0,549
91,422	3,420	1,385	0,758	1,265	0,099	0,176	0,809	0,133	0,183
90,886	3,647	1,455	0,815	1,168	0,166	0,196	0,957	0,126	0,209
88,061	5,007	2,658	0,801	0,940	0,398	0,209	1,078	0,092	0,182
81,263	4,044	11,166	0,415	0,361	1,874	0,250	0,364	0,080	0,158
87,438	4,384	4,226	0,515	1,554	0,149	0,142	1,078	0,096	0,168
78,435	3,609	13,614	0,586	1,144	0,995	0,231	0,849	0,133	0,254

Table 2: Trace Elemental Compositions.

Ag	As	Mo	Nb	Ni	Sn	Ta	Tl	W	Ba	Co	Cr	Cs	Cu	Li	Ga	Hf	Nb	Rb	Sc	Sr	U	V	Y	Zr	Th
0,01	1,1	0,99	10,2	7,9	1,3	1,12	0,26	0,4	710	2,5	188	1,43	6,1	13,4	7,96	2,8	10,2	46,1	2,5	64,5	696	41	17,2	121	10,7
0,02	0,2	1,16	5,8	7,3	0,9	0,59	0,31	0,3	960	2,8	162	0,92	3	11,8	8,44	1,9	5,8	62,3	2,4	90,8	286	45	9,5	65	4,75
0,01	1,6	1,17	5	4,8	0,8	0,4	0,16	0,3	390	0,8	155	0,46	3,3	7	3,66	1,6	5	31,4	0,8	54,6	201	22	8,3	54,9	7,18
0,06	18,9	0,82	21,8	9,4	3	1,45	0,55	0,8	560	6,1	20	5,82	6,4	28	14,75	3,4	21,8	120,5	3,3	89,9	153	241	17,6	116	12,8
0,02	3,2	0,33	6,5	3,3	0,9	0,61	0,29	0,3	1260	2,3	5	1,08	2,2	6,4	5,92	1,5	6,5	59,5	2,3	86,3	80,5	56	9,7	50,4	5,51
0,01	4,4	0,39	5,6	2,8	0,9	0,49	0,26	0,3	580	1,9	5	1,04	2,6	6,9	5,56	1,4	5,6	56,9	2,4	81,2	59,6	56	8,5	47,6	5,85
0,02	3,2	0,24	8,2	6	1,3	0,66	0,39	0,4	690	3,3	12	1,89	1,8	34,1	12,85	2	8,2	88,6	3,1	95,1	230	146	13,5	65,6	5,56
0,03	4,5	0,31	9,9	5,9	1,4	0,74	0,39	0,6	710	4,2	11	1,85	2,1	28,6	12,25	2	9,9	87,2	6,1	123,5	314	138	17,3	70,6	6,6
0,02	2,6	1,09	4,6	8	0,9	0,44	0,25	0,4	510	1,8	232	1,01	14,1	16,4	6,39	1,6	4,6	55,4	1,5	73,4	77	67	7,1	47,2	5,4
0,01	1,7	1,06	21,6	6,1	2,2	1,33	0,11	1,3	140	1,5	179	95,6	4,3	14	11,4	3,7	21,6	24,8	2,5	23,9	121,5	56	15,5	131	6,78
0,01	1,3	0,3	16,6	2,7	3	1,15	0,13	1,5	170	1,4	16	49,9	5,4	16,8	7,9	3,9	16,6	30,2	2,9	21,3	753	31	29,4	137,5	7,71
0,03	2,5	0,53	14,1	4,2	7,8	1,43	0,08	0,8	100	2	11	48,1	13,2	15,7	7,03	3,9	14,1	18,9	2,4	18,8	286	48	21,9	134,5	9,48
0,04	4,9	0,69	28,5	12,3	3	1,64	0,19	1,4	210	7,3	106	142,5	21,2	59,3	23,3	3,8	28,5	41,4	8,3	155	332	219	29,7	137,5	21,8
0,04	21,1	0,5	29,2	12,4	3,5	1,84	0,65	1	800	10,6	23	106	4,1	24,5	18,95	3,9	29,2	128,5	5,2	107,5	69,7	186	18,5	128	19,8
2,51	744	32,7	73,6	2,1	7,8	0,41	0,23	142,5	880	1,3	1	1,38	75,7	41,7	5,84	69,4	73,6	41,7	84,6	250	10000	987	500	500	4,77
6,47	807	24,2	66,8	5,6	7,6	0,43	0,21	137,5	910	1,7	131	1,66	515	56,3	5,92	65,4	66,8	38,1	97,3	220	10000	887	500	500	5,07
21,5	820	20,6	51,1	16,4	5,4	0,66	0,24	66,5	1620	39,1	1	7,5	1790	81,2	8,02	45,3	51,1	41,5	59	182	10000	581	500	500	6,09
6,2	756	22,2	49,5	16,8	4,8	0,47	0,07	94	4390	19,8	1	17,3	168	211	8,88	42,6	49,5	32,1	48,5	451	10000	635	470	500	5,29
2,53	732	18,25	48,8	15,2	5,1	0,57	0,37	65,7	1390	17,2	1	1,85	844	39,9	6,76	47,9	48,8	52,1	48,4	232	10000	612	419	500	6,26
2,26	745	22,2	71,8	16,9	6,8	0,94	0,19	104	2550	9,7	1	5,78	1310	119	8,03	69,2	71,8	51	79,6	518	10000	849	500	500	8,51

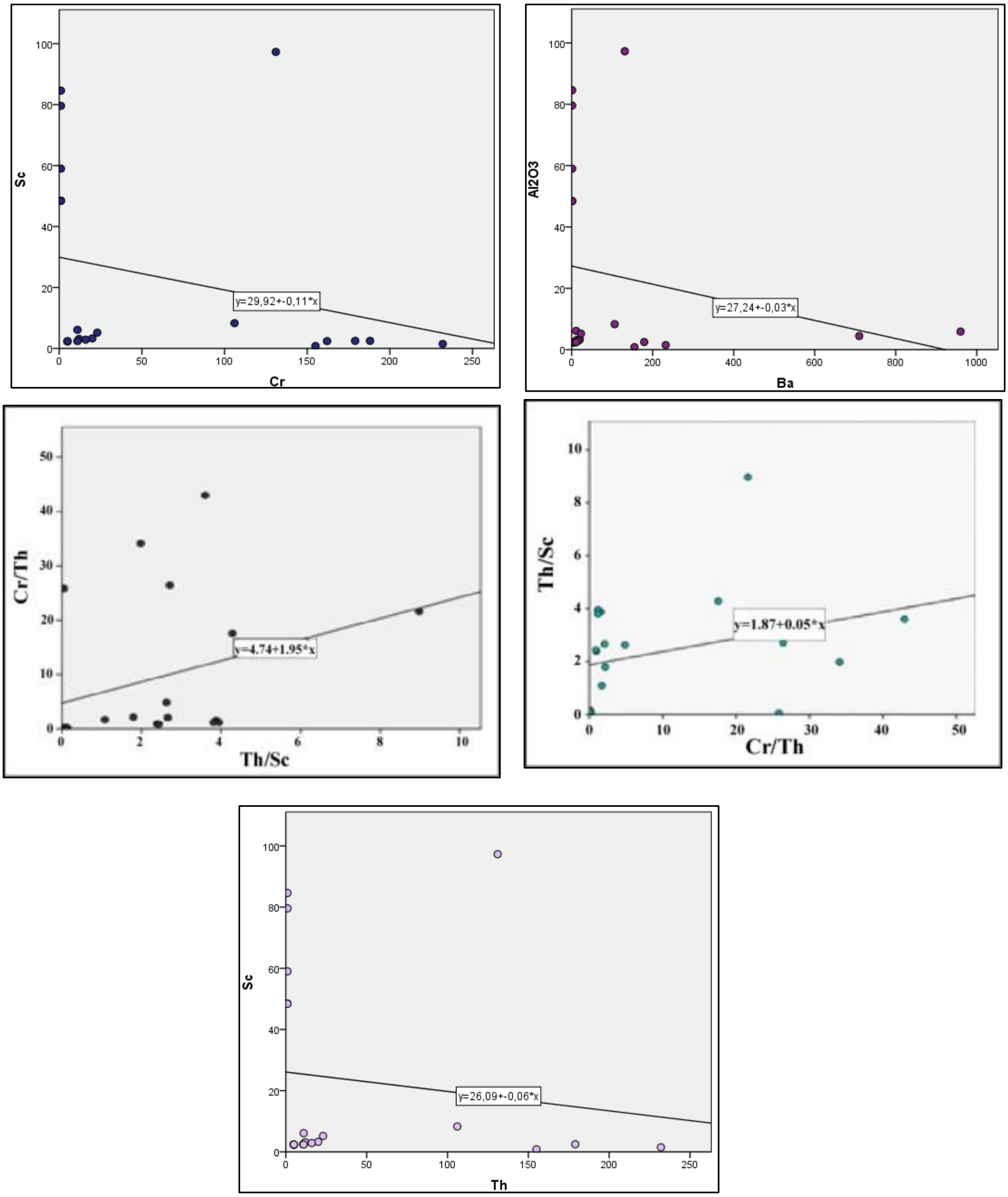

Figure 4: Bivariate correlation plots of the trace elements for the study area.

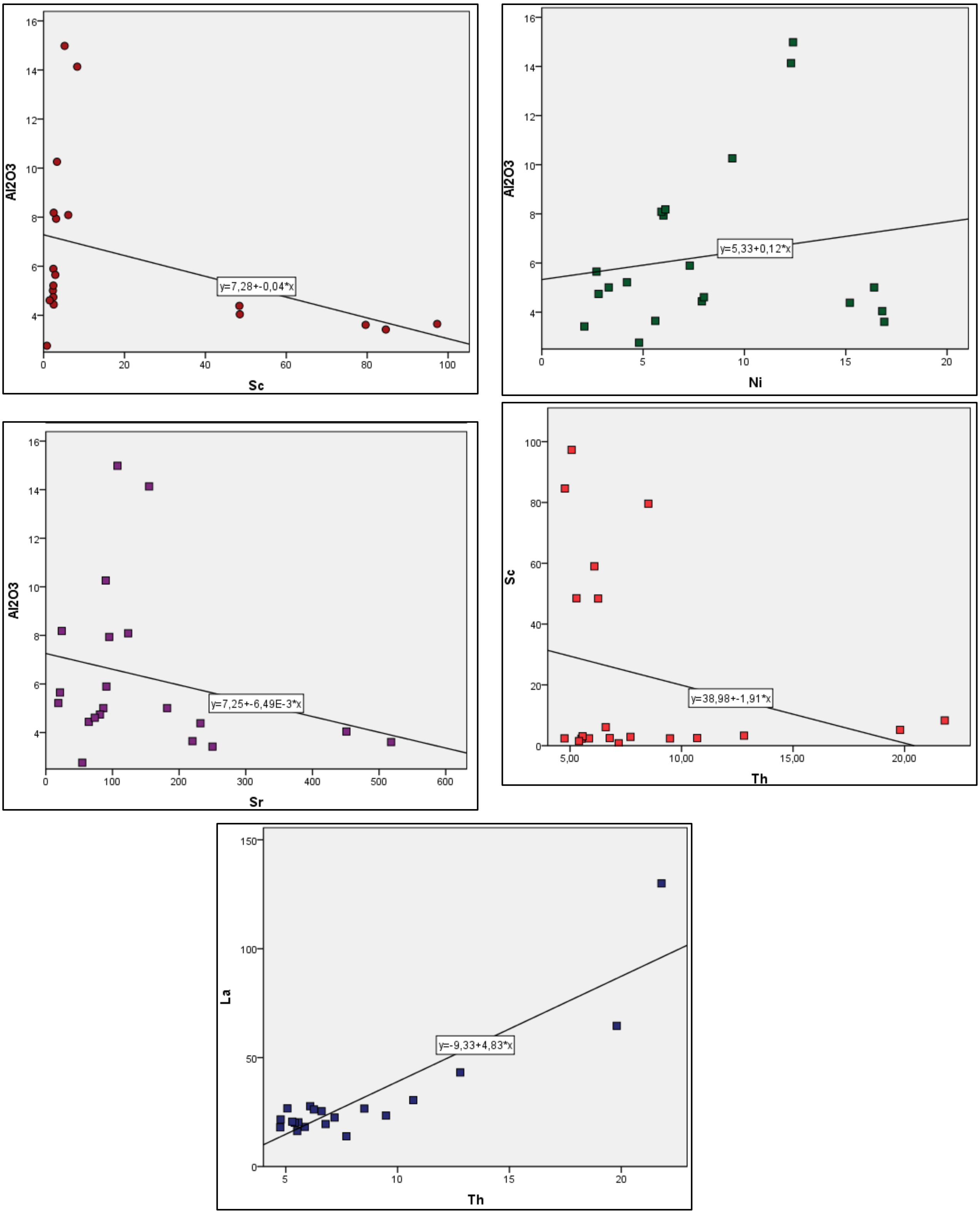

Figure 5: Bivariate correlation plots of the trace elements for the study area.

3) Rare Earth Elements Geochemistry

The REE are among the least traceable elements and are relatively immobile during low grade metamorphism, weathering and hydrothermal alteration. They are an effective indicator of sediment sources when compared with the upper continental crust, oceanic crust and mantle minerals. The pathway followed by elements during weathering and subsequent deposition as sediment is best understood by the behavior often revealed by the REE in authigenic and biogenic sedimentary phase and seawater. The distribution of REE in seawater often reveals their fractionation in sediments while their concentration in rivers reveals their removal from seawater by authigenic and biogenic phrase resulting in decrease in their total concentration [25]. The concentration of REE in sediments result from completing influences of the provenance, weathering, diagenesis, sediment sorting and the aqueous geochemistry of the individual elements [26]. The REE Chondrite Normalizing factor was used [27]. Other normalized plots and parameters used to characterize REE abundance includes:

1. Eu/Eu* anomaly which is the ratio of actual normalized Eu to interpolated normalized Eu for non-depletion or enrichment of the chondrite-normalised plots and is calculated by the following equation: $Eu/Eu^* = \sqrt{Eu_N/(Sm_N \times Gd_N)}$,
2. $Ce/Ce^* = 5Ce_N/[4La_N + Sm_N]$.

Note: N and * indicate chondrite normalized elements.

In the study area, the concentration of REE is highly variable with appreciable enrichment in LREE (La to Sm) over the HREE (Gd to Lu) (**Fig. 6**). Eu/Eu* is used to evaluate the abundance of plagioclase and negative Eu anomalies denote felsic source rocks. In the studied area Eu anomalies indicate that all samples are from felsic rocks. According to the Ce/Ce*, all studied samples show values ranging from 0.665 to 1.110. This suggests that the studied samples were deposited in relatively oxidizing environments.

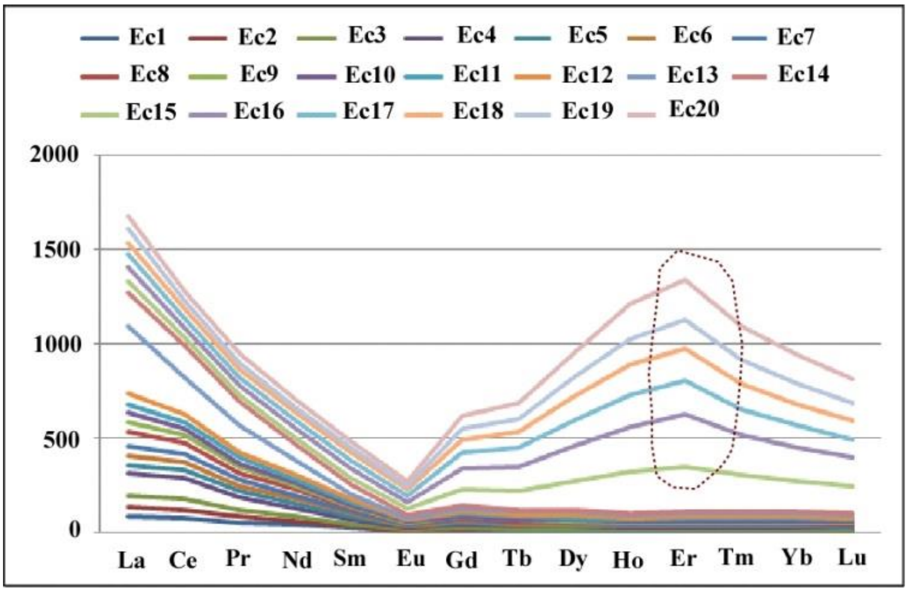

Figure 6: Chondrite-normalized REE patterns of Triassic sandstones of the DASA graben.

4) *Source area Weathering and Paleo- Redox Conditions*

According to [28], the weathering history of ancient sedimentary rocks can be evaluated in part by examining relationships among the alkali and alkaline earth elements. This is because alteration of igneous rocks during weathering results in depletion of alkali and alkaline earth elements and preferential enrichment of Al_2O_3 and SiO_2. In this study we use the Chemical Index of Alteration (CIA), Plagioclase Index of Alteration (PIA) and Chemical Index of Weathering (CIW) proposed by [29] [30] [31] [32].

The CIA, PIA and CIW values are respectively ranged from 18.78% - 69.01%, 14.56% - 80.26% and 19.97% - 84.51% with an average of 55.798%, 60.45% and 67.30% respectively (Table 4). These values are variable and may be as a result of multiple provenances for the sediments which have variable proportions of source area weathering and related process or may be due to low concentration of the alkaline and alkaline earth elements. The PIA and CIW values are greater than 70% indicating moderate to intensive weathering either at the source or during transport before deposition. The CIA, PIA and CIW values that are lesser than 70% indicate low weathering sources.

In order to infer the paleo-oxygenation conditions of the studied samples the U/Th ratio has been used as a redox indicator [33] [35] [36] [37]. According to [33] [34] [35] [37] [38] U/Th ratio below 1.25 suggests oxic deposition conditions whereas values above 1.25 suggest suboxic and anoxic conditions. In this study, all samples had high U/Th > 1.25 ratios, indicating that the studied samples were deposited in an anoxic environment. Moreover, the Th/U ratios have been used to evaluate the uranium enrichment of the Tarat formation compared to the crust average compositions. According to [7] the Th/U > 4 indicates uranium depletion over the crust composition while Th/U < 3 (ranging from 0.0004 to 0.2840) indicates the uranium enrichment over the crust average composition. The present study indicates that all samples had Th/U < 3 suggesting very high uranium enrichment in the studied area. This is also an indication of intense weathering in the source areas or sediments recycling.

5) Provenance Indices

Several classifications have been proposed to discriminate sediments into various tectonic settings [39] [11] [40]. The provenance signatures employed in this study have distinguished the sources of the sediments into four provenance zones: mafic, intermediate or felsic, igneous and quartzose sedimentary. The discriminant functions of the two plots used to discriminate the sediments within the study area are based on: **Discriminant Function 1 =** $(-1.773 \times TiO_2\%) + (0.607 \times Al_2O_3\%) + (0.76 \times Fe_2O_3T\%) + (-1.5 \times MgO\%) + (0.616 \times CaO\%) + (0.509 \times Na_2O\%) + (-1.22 \times K_2O\%) + (-9.09)$; **Discriminant Function 2** = $(0.445 \times TiO_2\%) + (0.07 \times Al_2O_3\%) + (-0.25 \times Fe_2O_3T\%) + (-1.142 \times MgO\%) + (0.432 \times Na_2O\%) + (1.426 \times K_2O\%) + (-6.861)$.

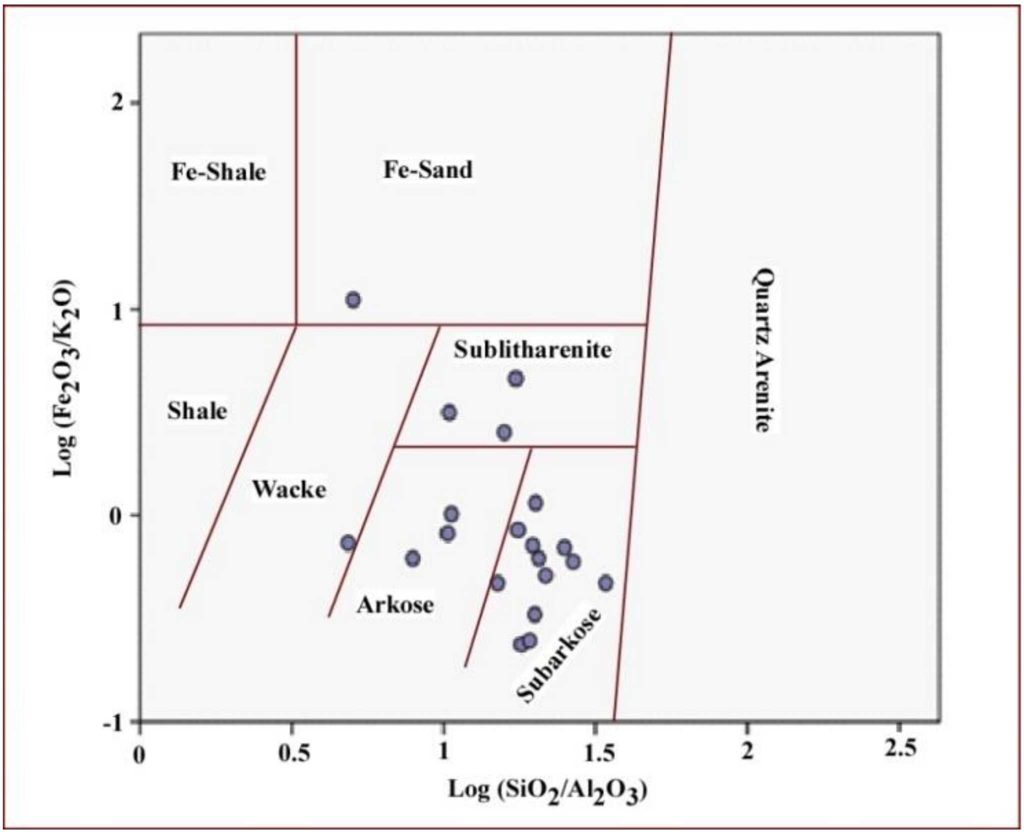

Figure 7: Geochemical classification of studied samples, using bivariate diagram Log (Fe_2O_3/K_2O) versus log (SiO_2/Al_2O_3) after [41].

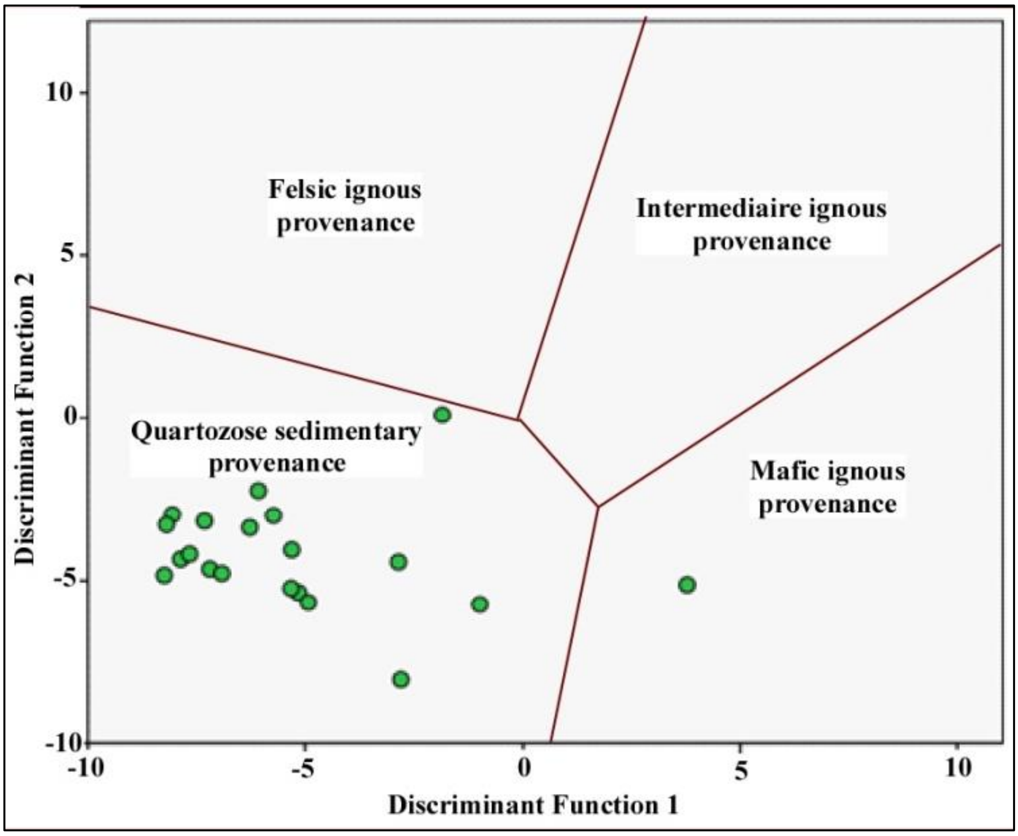

Figure 8: Provenance discrimination diagram for the studied samples after [42].

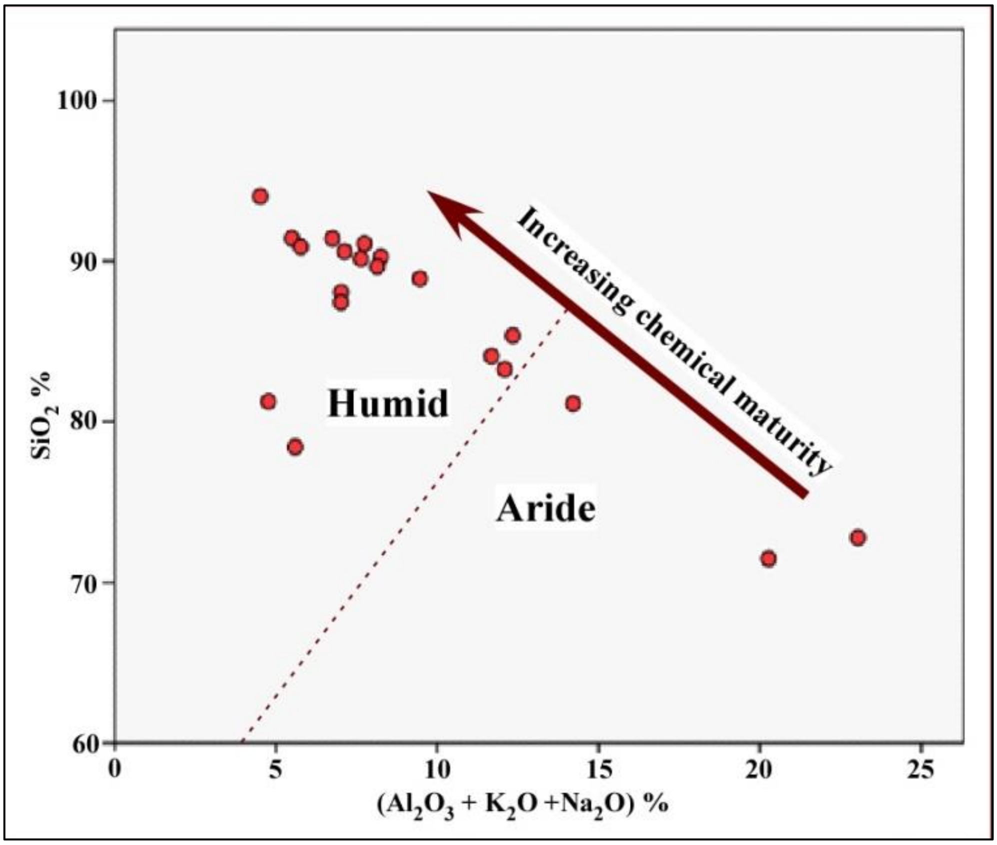

Figure 9: Depositional environmental climatic conditions of the studied samples based on SiO_2 wt.% versus (Al_2O_3 + K_2O + Na_2O) wt.% bivariate diagram after [43].

6) Tectonic Setting

The authors in [20] [42] [44] [45] [46] have demonstrated that the chemical compositions of sedimentary rocks are significantly controlled by plate tectonic settings of their provenances depositional basins and have introduced a discrimination diagram utilizing K2O/Na2O versus SiO2 to determine the tectonic setting of terrigenous sedimentary rocks. The plot K2O/Na2O versus SiO2 for the study samples (**Fig. 10**) implies that most of the samples are typical of sediments deposited in a passive margin setting, while 6 samples are derived from Active Continental Margin. According to the authors in [42] passive margin sediments are largely quartz-rich sediments derived from plate interiors or stable continental areas and deposited in intra cratonic basins or on passive continental margins.

Also, the discrimination diagram (log (K2O/Na2O) vs (SiO2)) shows that most of the sediments are of the passive margin with a 6 active continental margin sources (**Fig. 11**) [40].

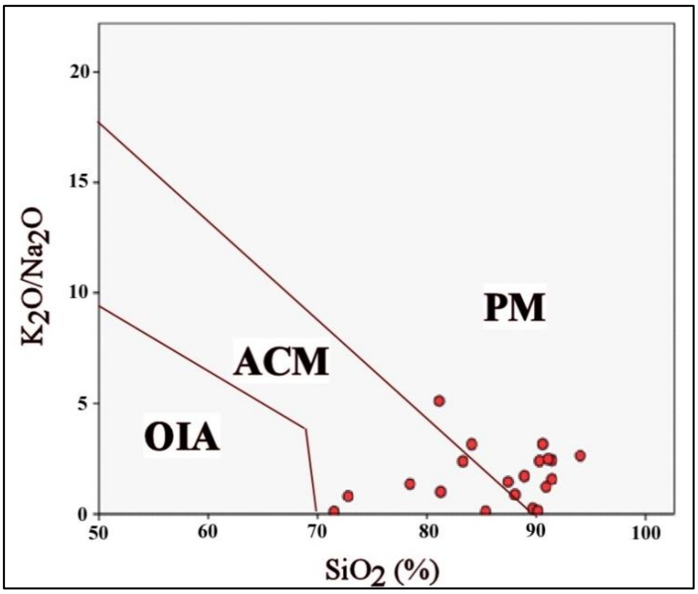

Figure 10: SiO_2 wt.% versus K_2O/Na_2O diagram: ACM = Active Continental Margin, OIA = Oceanic Island Arc and PM = Passive Margin [42].

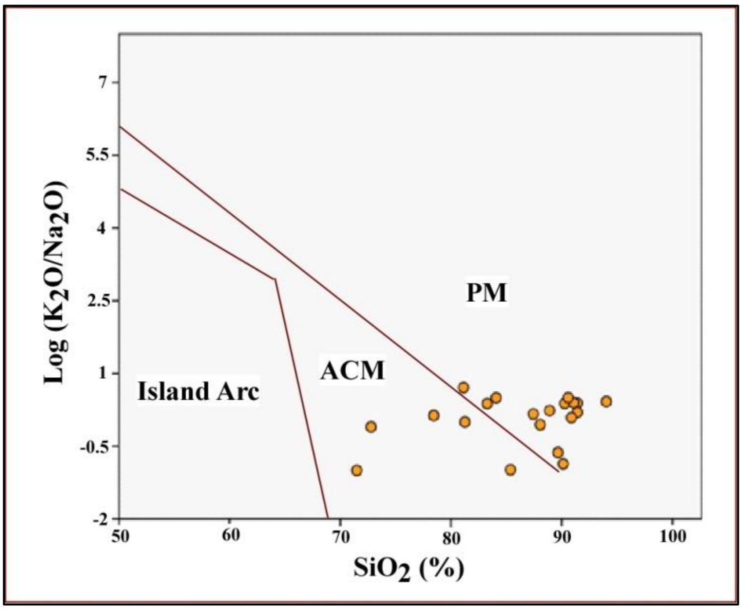

Figure 11: Tectonic discriminant diagram for the study areas [40].

7) *Uranium Mineralization and Associated Elements*

The purpose of using factor analysis of geochemical data in this research is to group the elements associated or not with uranium and those representing the detrital fraction. Furthermore, the correlational analysis is used to determine the genesis of uranium mineralization. As such, we classified the samples into two groups in accordance with their uranium contents:

- Samples with U < 500 ppm and;
- Samples with U > 500 ppm.

i. *Relationship between U and Major Elements*

a) Samples with U > 500 ppm

In order to study the relationship between U and the major elements we have first proceeded to the spatial representation in a three dimensional diagram (**Fig. 12**). The factor analysis results of samples with U > 100 ppm are represented in the three-dimensional spatial diagram and reflect the distribution of the elements in three factors after rotation (**Fig. 12**).

Three factors selected in this analysis express 87.75% of the total variance are divided as such: factor 1 (**53.06%**), factor 2 (**23.59%**) and factor 3 (**11.10%**). In order to visualize and distinguish the different poles, two factors 1 and 2 have been used since they formed to **76.65%** of the total variance. The two-dimensional spatial diagram (**Fig. 13**) of factors 1 and 2 distinguished several poles:

- The siliceous SiO2 pole which corresponds mineralogically to the fraction of detrital grains of quartz ;
- Uraniferous pole including U, Mo, Pb, V, Zn, As, Nb and P_2O_5 close and distinct to the organic pole but anticorrelated to the siliceous pole. The uraniferous pole extends towards the siliceous pole suggesting double sources of these elements such as detrital provenance and precipitation with mineralization;
- Pole controlled by carbonate (CaO) associated with Ba, MnO, MgO, Sr, Cu and Co ;
- Pole controlled by K_2O associated by La and Rb,
- Pole controlled by aluminum associated by, Fe_2O_3, TiO_2, Na_2O and Th.

Data from **Table 3** show a negative correlation between uranium and SiO_2, Al_2O_3, Fe_2O_3, Na_2O and TiO_2. Positive correlations are definite with uranium and others major oxides. Also, negative correlations are observed with SiO_2 and CaO, MgO, MnO, P_2O_5 and TiO_2 while positive correlations are observed with SiO_2 and others major oxides. These relationships may be explained by:

- According to mineralization: uranium is associated with a strong depletion of alkaline oxides or mineralization occurs in altered host environments depleted of these oxides.
- The negative correlation between SiO_2 and some major oxides can reflect the dilution effect of quartz in these samples.

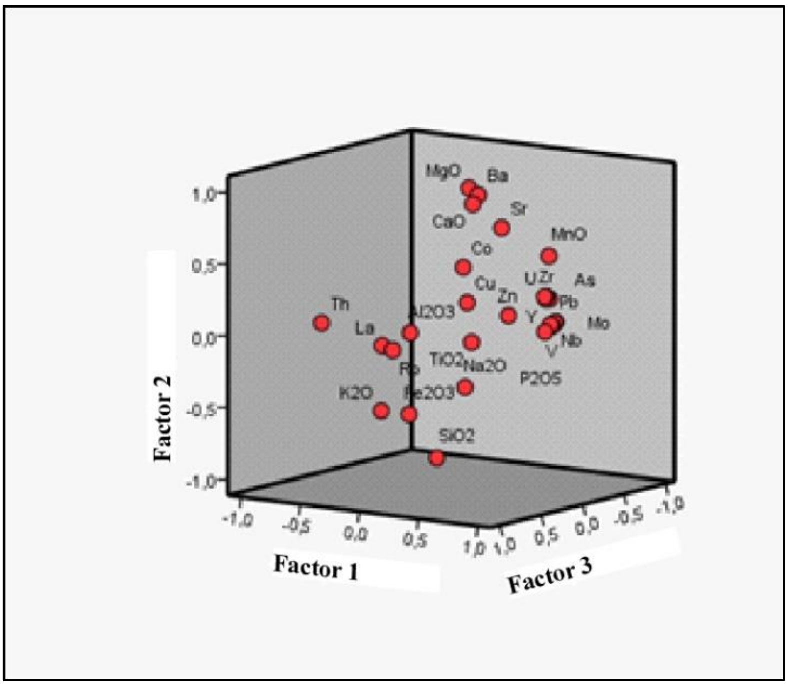

Figure 12: 3D spatial diagram plot of factors 1, 2 and 3 of samples with U > 500 ppm.

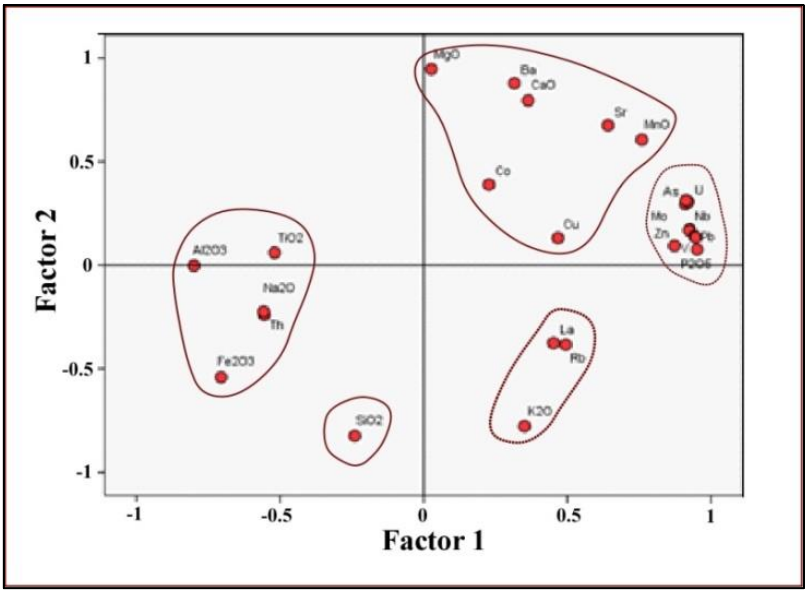

Figure 13: 2D spatial diagram of factors 1 and 2 of samples with U > 500 ppm.

b) Samples with U < 500 ppm

Also for U < 500 ppm three factors are selected to visualize the elements distribution in three-dimensional spatial diagram (**Fig. 14**). The three factors selected in this analysis express 87.75% of the variance (factor 1 : **56.63%** ; factor 2 : **19.08%** ; factor 3 : **12.46%**). In order to visualize and distinguish the differents poles, factor 1 and 2 have been used since they formed **65.71%** of the total variance. Several poles have been distinguished (**Fig. 15**) in this two-dimensional spatial diagram.

- The siliceous SiO2 pole ;
- Uraniferous pole including U, Ba, Pb, Sr associated with Na_2O close ;
- Pole controlled by carbonate (CaO) associated with MnO, MgO, Fe_2O_3, Al_2O_3, K_2O, P_2O_5 and TiO_2 including Y, V, Co, Zn, Zr, La, Nb and Th ;
- Pole controlled by Cu associated by Mo.

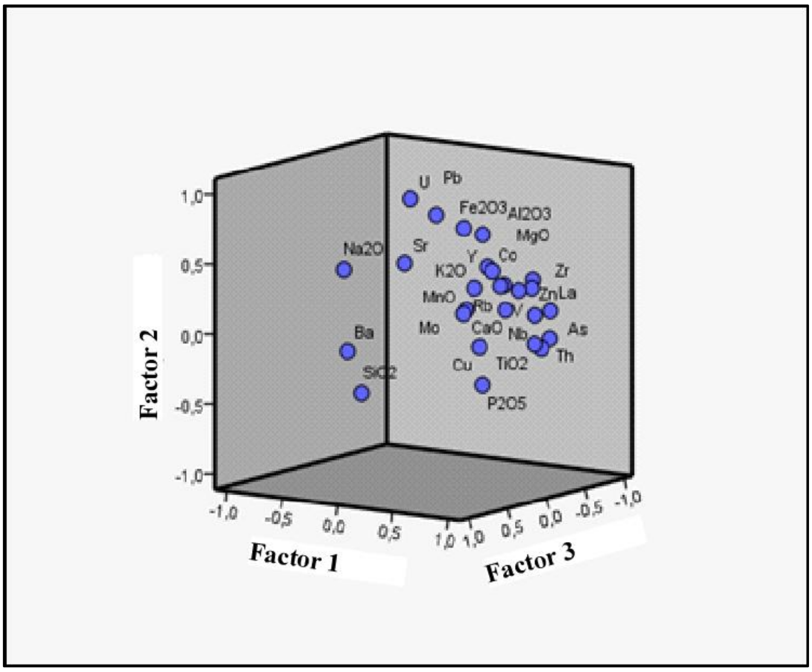

Figure 14: 3D spatial diagram plot of factors 1, 2 and 3 of samples with U < 500 ppm.

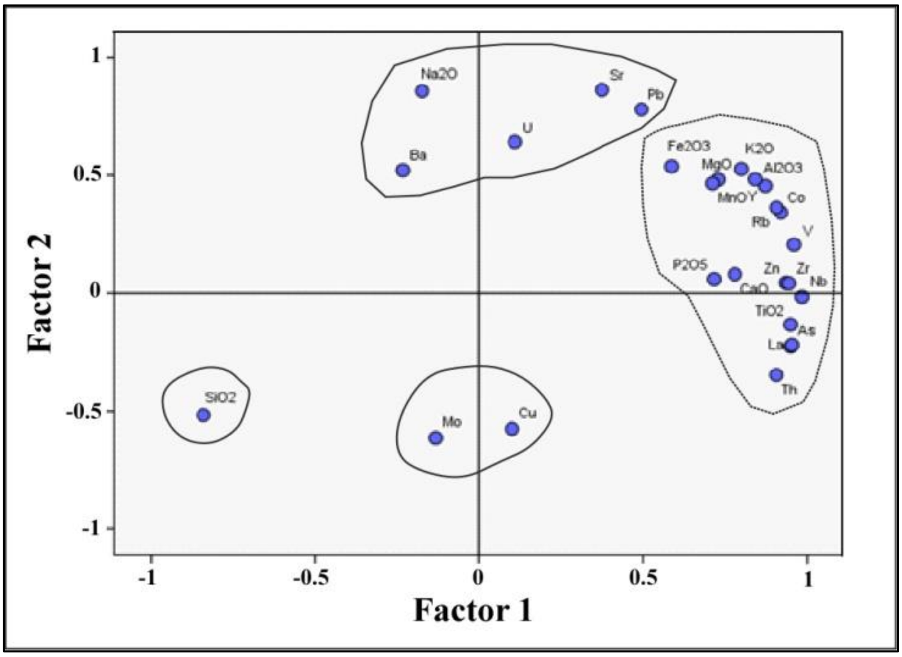

Figure 15: 2D spatial diagram of factors 1 and 2 of samples with U < 500 ppm.

Data from **Table 4** show positive correlations between U and major oxides except SiO_2 and K_2O. These suggest that uranium mineralization under 500 ppm occurs in an altered environment. Negative correlations are observed with SiO_2 and all major oxides. These negative correlations reflect the "dilution effect" of quartz in Triassic formations.

Table 2: Results of Correlation Analysis between U > 500 ppm and Major Oxides of studied Samples.

	SiO2	**Al2O3**	**CaO**	**Fe2O3**	**K2O**	**MgO**	**MnO**	**Na2O**	**P2O5**	**TiO2**	**U**
SiO2	1,000										
Al2O3	,230	1,000									
CaO	-,984	-,395	1,000								
Fe2O3	,666	,579	-,750	1,000							
K2O	,358	-,360	-,289	,002	1,000						
MgO	-,816	-,160	,821	-,586	-,618	1,000					
MnO	-,618	-,542	,683	-,780	-,302	,551	1,000				
Na2O	,326	,720	-,456	,671	-,240	-,489	-,475	1,000			
P2O5	-,294	-,777	,404	-,618	,183	,041	,799	-,376	1,000		
TiO2	-,049	,451	-,061	,574	-,414	-,135	-,290	,823	-,252	1,000	
U	-,405	-,620	,496	-,816	,016	,257	,917	-,470	,903	-,452	1,000

Table 4: Results of Correlation Analysis between U < 500 ppm and Major Oxides of studied Samples.

	SiO2	**Al2O3**	**CaO**	**Fe2O3**	**K2O**	**MgO**	**MnO**	**Na2O**	**P2O5**	**TiO2**	**U**
SiO2	1,000										
Al2O3	-,993	1,000									
CaO	-,044	,022	1,000								
Fe2O3	-,848	,786	-,030	1,000							
K2O	-,221	,245	,440	-,072	1,000						
MgO	-,860	,810	,231	,924	,218	1,000					
MnO	-,685	,634	,502	,698	,316	,791	1,000				
Na2O	-,776	,782	-,408	,683	-,336	,493	,279	1,000			
P2O5	-,784	,744	-,054	,850	-,186	,683	,631	,749	1,000		
TiO2	-,825	,857	-,034	,613	-,123	,561	,430	,841	,739	1,000	
U	-,195	,121	,098	,497	-,302	,475	,312	,171	,236	,003	1,000

ii. Relationship between U and Trace Elements

a) Samples with U > 500ppm

Table 5 shows positive correlation between U and all trace elements excepted Cr and Th who show a negative correlation with U. These negative correlations suggest close affiliation of uranium minerals, chrome and thorium or common origin and similar geochemical composition of these elements.

b) samples with U < 500ppm

Table 6 shows negative correlation between U and Ce, As, Mo and Ba. This reflects close affiliation of uranium minerals and Cr, As, Mo and Ba. Moreover, there is a positive correlation between U and V, Co, Ni, Cu, Zn,Zr, Ag, Pb and Th.

Table 5: Results of Correlation Analysis between U > 500 ppm and Trace Elements of studied Samples.

	V	Cr	Co	Ni	Cu	Zn	As	Zr	Mo	Ag	Ba	Pb	Th	U
V	1,000													
Cr	-,363	1,000												
Co	,100	-,453	1,000											
Ni	,179	-,361	,762	1,000										
Cu	,341	-,367	,747	,683	1,000									
Zn	,859	-,432	,050	,265	,337	1,000								
As	,909	-,467	,475	,480	,566	,719	1,000							
Zr	,918	-,512	,445	,480	,536	,754	,996	1,000						
Mo	,974	-,432	,209	,189	,313	,834	,921	,927	1,000					
Ag	,231	-,242	,856	,440	,718	,014	,517	,455	,327	1,000				
Ba	,340	-,389	,458	,745	,199	,336	,506	,521	,388	,212	1,000			
Pb	,993	-,385	,144	,206	,417	,874	,906	,911	,966	,285	,331	1,000		
Th	-,692	,490	-,235	,032	-,079	-,346	-,737	-,737	-,767	-,382	-,241	-,648	1,000	
U	,918	-,499	,445	,485	,537	,758	,996	1,000	,928	,455	,524	,911	-,729	1,000

Table 6: Results of Correlation Analysis between U < 500 ppm and Trace Elements of studied Samples.

	V	Cr	Co	Ni	Cu	Zn	As	Zr	Mo	Ag	Ba	Pb	Th	U
V	1,000													
Cr	-,360	1,000												
Co	,837	-,332	1,000											
Ni	,759	,181	,846	1,000										
Cu	,278	,297	,203	,475	1,000									
Zn	,895	-,187	,775	,802	,496	1,000								
As	,733	-,405	,820	,613	-,045	,574	1,000							
Zr	,502	-,103	,549	,564	,468	,606	,433	1,000						
Mo	-,299	,887	-,272	,189	,202	-,056	-,191	,026	1,000					
Ag	,860	-,370	,754	,671	,345	,837	,769	,563	-,162	1,000				
Ba	-,024	-,293	,122	-,117	-,575	-,191	,136	-,567	-,310	-,013	1,000			
Pb	,730	-,112	,738	,759	,512	,854	,287	,470	-,180	,537	-,090	1,000		
Th	,736	-,164	,863	,824	,544	,839	,641	,730	-,092	,681	-,263	,803	1,000	
U	,168	-,027	,034	,129	,309	,400	-,324	,254	-,010	,201	-,273	,498	,141	1,000

iii. Relationship between U and REE

a) Samples with U > 500ppm

There is a positive correlation with uranium and REE except Ce (**r = - 0.248**) (**Table 7**). The positive correlation between U and these REE indicates the similar geochemical composition of these elements during mineralization.

Table 7: Results of correlation analysis between U > 500 ppm and trace elements of Triassic samples

	La	Ce	Pr	Nd	Sm	Eu	Gd	Tb	Dy	Ho	Er	Tm	Yb	Lu	U
La_ppm	1,000														
Ce_ppm	,830	1,000													
Pr_ppm	,889	,920	1,000												
Nd_ppm	,744	,596	,853	1,000											
Sm_ppm	,369	,044	,414	,823	1,000										
Eu_ppm	,249	-,141	,236	,695	,973	1,000									
Gd_ppm	,254	-,169	,199	,660	,958	,993	1,000								
Tb_ppm	,226	-,192	,176	,639	,950	,991	,998	1,000							
Dy_ppm	,229	-,202	,164	,613	,930	,978	,989	,995	1,000						
Ho_ppm	,218	-,207	,158	,594	,911	,962	,973	,984	,996	1,000					
Er_ppm	,225	-,204	,156	,585	,898	,950	,966	,977	,992	,998	1,000				
Tm_ppm	,211	-,219	,137	,558	,876	,936	,952	,967	,986	,996	,998	1,000			
Yb_ppm	,215	-,217	,137	,553	,869	,930	,946	,962	,983	,994	,997	1,000	1,000		
Lu_ppm	,207	-,219	,137	,556	,874	,932	,948	,963	,984	,995	,998	,999	1,000	1,000	
U_ppm	,235	-,248	,087	,486	,797	,895	,900	,910	,925	,926	,919	,929	,930	,919	1,000

To better understand the relationship between U and REE, the results of factor of samples with U > 500 ppm are represented in the three-dimensional spatial diagram and reflect the distribution of the elements in three factors after rotation (**Fig. 16**). Three factors selected in this analysis express a total variance of **85.46%**, as such factor 1 (**71.21%**), factor 2 (**21.85%**) and factor 3 (**2.40%**). For more visualization of poles two factors 1 and 2 that have **83.06%** of the total variance are used. The two-dimensional spatial diagram of factors 1 and 2 has distinguished two poles:

- Uraniferous pole,
- And pole with all REE.

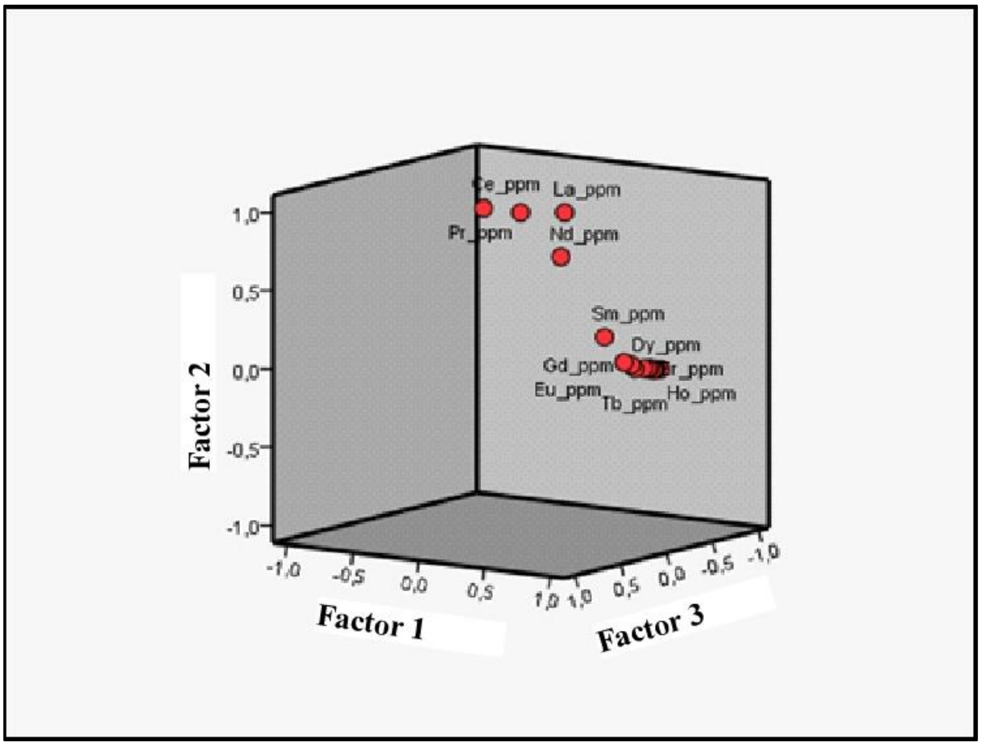

Figure 16: 3D spatial diagram plot of factors 1, 2 and 3 of REE of samples with U > 500 ppm.

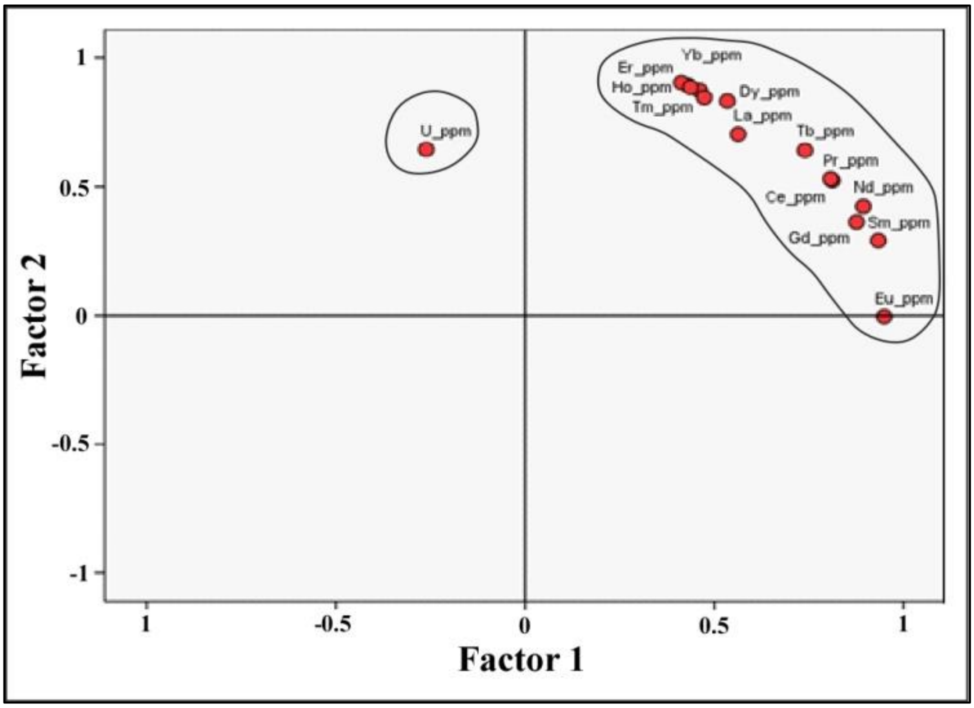

Figure 17: 2D spatial diagram plot of factors 1, 2 and 3 of REE of samples with U > 500 ppm.

b) Samples with U < 500ppm

Table 8 shows positive correlation between U and REE except Sm, Eu and Gd. The positive correlation with U and these elements suggests the similar geochemical composition of these elements during mineralization.

Table 8: Results of correlation analysis between U < 500 ppm and trace elements of Triassic Samples.

	La	Ce	Pr	Nd	Sm	Eu	Gd	Tb	Dy	Ho	Er	Tm	Yb	Lu	U
La_ppm	1,000														
Ce_ppm	,928	1,000													
Pr_ppm	,933	,995	1,000												
Nd_ppm	,839	,977	,977	1,000											
Sm_ppm	,656	,876	,870	,953	1,000										
Eu_ppm	,449	,725	,726	,843	,922	1,000									
Gd_ppm	,653	,855	,844	,925	,982	,874	1,000								
Tb_ppm	,818	,908	,905	,922	,912	,728	,942	1,000							
Dy_ppm	,887	,867	,867	,824	,753	,509	,802	,954	1,000						
Ho_ppm	,883	,811	,817	,750	,658	,403	,703	,900	,984	1,000					
Er_ppm	,884	,808	,812	,738	,637	,378	,677	,882	,975	,993	1,000				
Tm_ppm	,894	,828	,836	,767	,667	,416	,698	,895	,976	,992	,997	1,000			
Yb_ppm	,886	,817	,820	,749	,650	,392	,682	,882	,968	,988	,997	,996	1,000		
Lu_ppm	,870	,813	,822	,761	,672	,438	,691	,885	,955	,981	,986	,990	,992	1,000	
U_ppm	,319	,123	,118	,003	-,095	-,225	-,043	,209	,409	,483	,505	,465	,467	,438	1,000

Also, to better understand the relationship between U and REE, the results of factor of samples with U< 500 ppm are represented in the three-dimensional spatial diagram and reflect the distribution of the elements in three factors after rotation (**Fig. 18**). Three factors selected in this analysis expressed a total variance of **96.70%**, as such factor 1 (**78.41%**), factor 2 (1**2.91%**) and factor 3 (**5.48%**). For more visualization of poles two factors 1 and 2 that have combined **91.31%** of the total variance were used (**Fig. 19**). The two-dimensional spatial diagram of factors 1 and 2 has distinguished two poles:

- Pole of La associated with Pr, Ce and Nd ;
- and uraniferous pole with others REE. The relationship of U and these REE suggests that these elements ensure the control of uranium mineralization distribution during weathering.

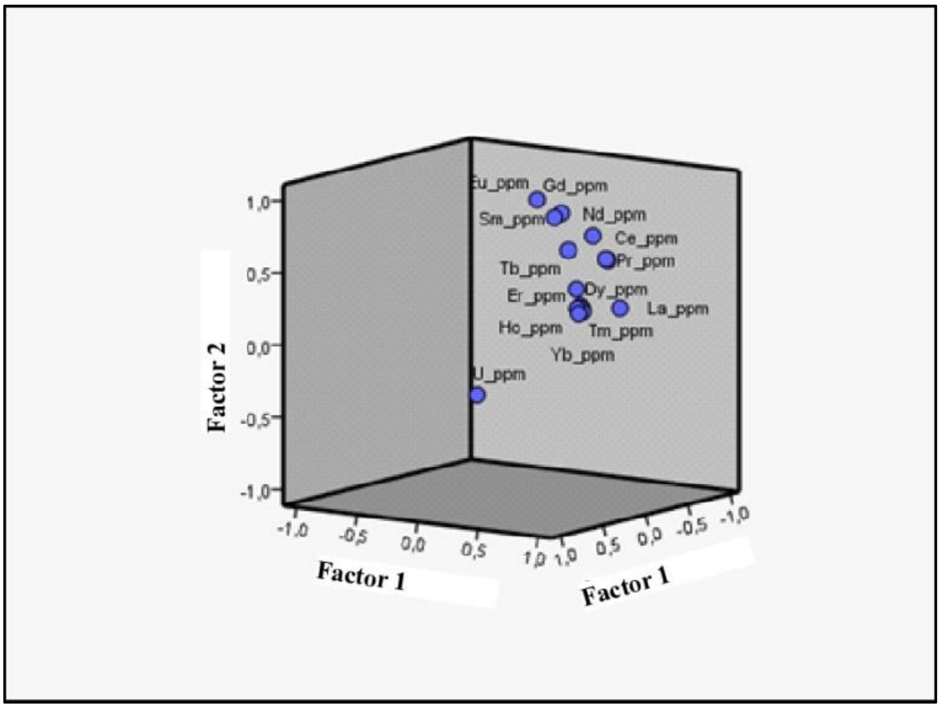

Figure 18: 3D spatial diagram plot of factors 1, 2 and 3 of REE of samples with U < 500 ppm.

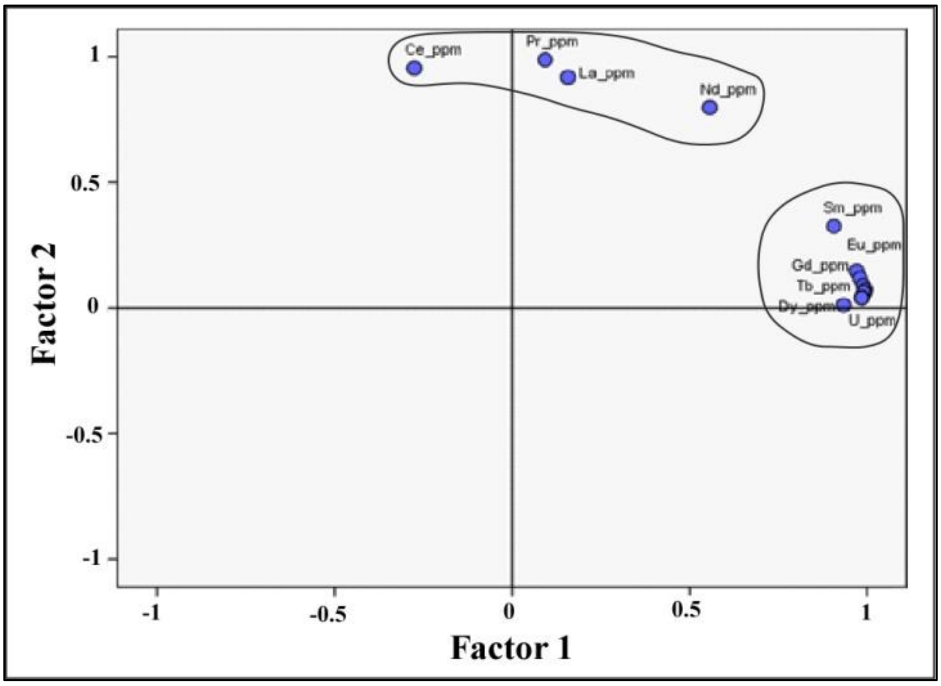

Figure 19: 3D spatial diagram plot of factors 1, 2 and 3 of REE of samples with U < 500 ppm.

E. Uranium genesis model for the Triassic formations of the DASA Graben

The studied Triassic sandstones of the DASA graben were derived from the erosion of the Aïr Mountains and reworking of older sediments. These sandstones were deposited in a continental fluvial to fluvio-deltaic sedimentary environment affected by passive margin (PM) and active continental margin (ACM).

Uranium mineralization in this area would have three origins:

- Uranium was leached during the weathering of the mafic rocks of the Aïr Mountains and transported and concentrated in the DASA graben ;
- Uranium was remobilized from Carboniferous, and Permian formations and concentrated in the Triassic formations ;
- Uranium would have been concentrated by fluid flows through the DASA graben faults. High grade uranium mineralization found in the sandstones was due to the intense fluid flows in this sector and along with the abundance of organic matter as well as analcime which fixed the uranium.

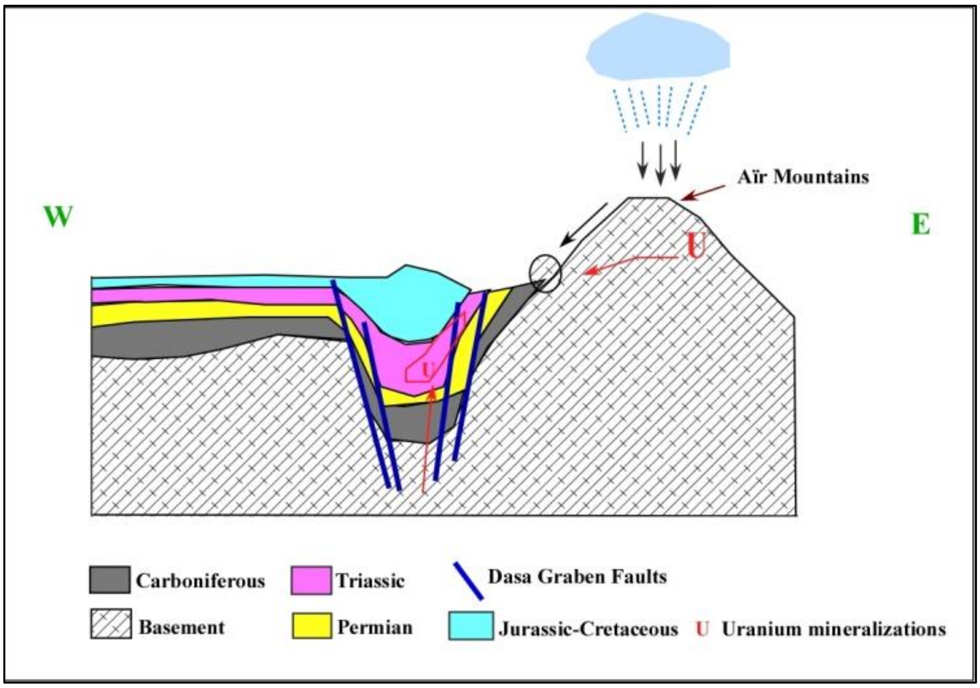

Figure 20: Genesis model of uranium deposit in Triassic formations, DASA graben.

V. CONCLUSION

The geochemical study of the DASA graben sandstone (Triassic formations) reveals that SiO_2 is the dominant major mineral followed by Al_2O_3 and Fe_2O_3 which together make up about 90% of the composition of the sediments while the other major elements such as K_2O, TiO_2, CaO, MgO and P_2O_5 constitute the remaining percentage. The CIA, CIW and PIA parameters indicate variable proportion of source area weathering and related process while the discrimination diagram (log (K2O/Na2O) vs (SiO2)) shows that most of the sediments are of the passive margin with an active continental margin sources. In this study, all samples had high U/Th > 1.25 ratios, indicating that the studied samples were deposited in an anoxic environment. The Th/U > 4 indicates uranium depletion over the crust composition while Th/U < 3 (ranging from 0.0004 to 0.2840) indicates the uranium enrichment over the crust average composition. The present work indicates that all samples had Th/U < 3 suggesting very high uranium enrichment in this studied area. This is also an indication of intense weathering in the source areas and/or sediments recycling.

Acknowledgment

The authors of this paper are much grateful to Global Atomic Corporation for data provided. Special thanks are to Mr. Stephen Roman for his help and authorization for data used.

VI. REFERENCES

1. Forbes P (1989) Rôles des structures sédimentaires et tectoniques, du volcanisme alcalin régional et des fluides diagénétiqueshydrothermaux pour la formation des minéralisations à U-Zr-Zn-V-Mo d'Akouta (Niger). PhD dissertation, University of NancyForbes P (1989) Rôles des structures sédimentaires et tectoniques, du volcanisme alcalin régional et des fluides diagénétiqueshydrothermaux pour la formation des minéralisations à U-Zr-Zn-V-Mo d'Akouta (Niger). PhD dissertation, University of Nancy.
2. Gerbeaud O (2006) Evolution structurale du bassin de Tim Mersoï: Déformations de la couverture sédimentaire, relations avec la localisation des gisements uranifères du secteur d'Arlit (Niger). PhD dissertation, University of Paris-Sud, 270p.
3. Cavellec S. (2006). Evolution diagénétique du bassin de Tim Mersoï et conséquences pour la genèse des minéralisations uranifères dans les formations du Guézouman et du Tarat (district Arlit-Akokan, Niger). Thèse de Doctorat de l'Université de Paris-Sud, 463 p.
4. Mamane MM (2016) The Metallogenic System of the Uranium-deposits associated with the Arlit Fault (Tim Mersoï Basin, Niger): diagenesis, fluid circulation and metal enrichment mechanisms (U, Cu, V).nPhD dissertation, University of Lorraine.
5. GREIGERT, J. et POUGNET, R., 1967. Essai de description des formations géologiques de la république du Niger. Publication Direction des Mines et de la Géologie, Niger, n°3, 273 p.
6. Valsardieu C (1971) Etude géologique et paléogéographique du bassin de Tim Mersoï, région d'Agadès (République du Niger). PhD dissertation, University of Nice.
7. Wagani I (2007) Potentialités uranifères des sources volcaniques envisageables pour la formation des minéralisations de la région d'Arlit (Niger). PhD dissertation, University of Paris-Sud.
8. Moreau C, Demaiffe D, Bellion Y, Boullier AM(1994) A tectonic model for the location of Palaeozoic ring complexes in Aïr (Niger, West Africa). Tectonophysics 234:129–146.
9. Mamane M. M., Michel C., Etienne D., Rémi S., and Marc B. (2019) Cenozoic oxidation episodes in West Africa at the origin of the in situ supergene mineral redistribution of the primary uranium orebodies (Imouraren deposit, Tim Mersoï Basin, Northern Niger).
10. Pacquet A (1969) Analcimes et argiles diagénétiques dans les formations sédimentaires de la région d'Agadès (République du Niger. PhD dissertation, University of Strasbourg.
11. Yahaya M, Lang J (2000) Tectonic and sedimentary evolution of the Akokan Unit during Visean times in the Tim Mersoï Basin (Arlit région, Niger). J Afr Earth Sci 31:415–431.
12. Forbes, P., Pacquet A., Chantret F., Oumarou J., Pagel M. (1984) Métallogénie. Marqueurs du volcanisme dans le gisement d'uranium d'Akouta (République du Niger). C.R. Acad. Sci. Paris, 298, 647-650.
13. Forbes P, Dubessy J (1988) Characterization of fresh and altered Montroseite [V,Fe]OOH. A discussion of alteration processes. Phys Chem Miner 15:438–445.
14. Turpin, L., Clauer N., Forbes P., Pagel M., 1991. U-Pb, Sm-Nd and K-Ar systematics of the Akouta uranium deposit, Niger. Chemical geology, 87, 217-230.
15. Sempéré, T. (1981) Le contexte sédimentaire du gisement d'uranium d'Arlit (République du Niger). Thèse de doctorat, ENSMP, Paris, 382 pp.
16. Bigotte, G., Obellianne, J.M., 1968. Decouverte de mineralisations uraniferes au Niger. Miner. Depos. 3, 317–333.
17. Crook, K.A.W. (1974) Lithostratigraphy and Geotectonic: The Significance of Composition Variation in Flysch arenites (Graywackes). In: Dott, R.H. and Shaver, R.H., Eds., Modern and Ancient Geosynclinal Sedimentation, Society of Economic Paleontologists and Mineralogists, Tulsa, Okla, 304-310. https://doi.org/10.2110/pec.74.19.0304
18. Armstrong-Altrin, J.S., Lee, Y.I., Verma, S.P. and Ramasamy, S. (2004) Geochemistry of Sandstones from the Upper Miocene Kudankulam Formation, Southern India: Implications for Provenance, Weathering, and Tectonic Setting. Journal of Sedimentary Research, 74, 285-297. https://doi.org/10.1306/082803740285
19. Feng, R. and Kerrich, R. (1990) Geochemistry of Fine-Grained Clastic Sediments in the Archean Abitibi Greenstones Belt, Canada: Implications for Provenance and Tectonic Setting. Geochimica et Cosmochimica Acta, 54, 1061-1081. https://doi.org/10.1016/0016-7037(90)90439-R

20. Bhatia, M.R. and Crook, K.A. (1986) Trace Element Characteristics of Graywackes and Tectonic Setting Discrimination of Sedimentary Basins. Journal of Mineralogy and Petrology, 92, 181-193. https://doi.org/10.1007/BF00375292
21. McLennan, S.M., Hemming, S., McDaniel, D.K. and Hanson, G.N. (1993) Geochemical Approaches to Sedimentation, Provenance, and Tectonics. Special Papers, Geological Society of America, 21. https://doi.org/10.1130/SPE284-p21
22. Mclennan, S.M. (1989) Rare Earth Elements in Sedimentary Rocks: Influence of Provenance and Sedimentary Processes. Mineralogical Society of America Reviews in Mineralogy, 21, 169-200.
23. McLennan, S.M. (2001) Relationships between the Trace Element Composition of Sedimentary Rocks and Upper Continental Crust. Geochemistry, Geophysics, Geosystems, 2, 154-155. https://doi.org/10.1029/2000GC000109
24. Lopez, J.M.G., Bauluz, B., Fernandez-Nieto, C. and Oliete, A.Y. (2005) Factors Controlling the Trace-Element Distribution in Fine-Grained Rocks: The AlbianKaolinite-Rich Deposits of the Oliete Basin (NE Spain). Journal of Chemical Geology, 214, 1-19. https://doi.org/10.1016/j.chemgeo.2004.08.024
25. Piper, D.Z. (1974) Rare Earth Elements in the Sedimentary Cycle: A Summary. Journal of Chemical Geology , 14, 285-304. https://doi.org/10.1016/0009-2541(74)90066-7
26. Nesbitt, H.W. and Markovics, G. (1980) Chemical Processes Affecting Alkalis and Alkaline Earths during Continental Weathering. Geochimica et Cosmochimica Acta , 44, 1659-1666. https://doi.org/10.1016/0016-7037(80)90218-5
27. Wakita, H., Rey, P. and Schmitt, R.A. (1971) Abundances of the 14 Rare-Earth Elements and 12 Other Trace Elements in Apollo 12 Samples: Five Igneous and One Breccia Rocks and Four Soils. Proceedings of the Lunar Science Conference , 2, 1319.
28. Kogbe, C.A. (1991) Stratigraphy and Tectonic History of the Iullemeden Basin in West Africa. South African Journal of Geology , 94, 19-31.
29. Fedo, C.M., Nesbitt, H.W. and Young, G.M. (1995) Unraveling the Effects of Potassium Metasomatism in Sedimentary Rocks and Paleosols, with Implications for Paleoweathering Conditions and Provenance. Geology, 23, 921-924. https://doi.org/10.1130/0091-7613(1995)023<0921:UTEOPM>2.3.CO;2
30. Bakkiaraj, D., Nagendra, R., Nagarajan, R. and Armstrong-Altrin, J.S. (2010) Geochemistry of Sandstones from the Upper Cretaceous Sillakkudi Formation, Cauvery Basin, Southern India: Implication for Provenance. Journal of the Geological Society of India, 76, 453-467.https://doi.org/10.1007/s12594-010-0128-3
31. Harnois, L. (1988) The CIW Index: A New Chemical Index of Weathering. Sedimentary Geology, 55, 319-322. https://doi.org/10.1016/0037-0738(88)90137-6
32. Nesbitt, H.W. and Young, G.M. (1982) Early Proterozoic Climates and Plate Motions Inferred from Major Element Chemistry of Lutites. Nature, 299, 715-717. https://doi.org/10.1038/299715a0
33. Hallberg, R.O. (1976) A Geochemical Method for Investigation of Palaeoredox Conditions in Sediments: Ambio. Special Report, 4, 138-147.
34. Taylor, S.R. and McLennan, S.M. (1985) The Continental Crust: Its Composition and Evolution. Blackwell, Oxford, 312.
35. Gupta, S., Banerjee, R., Babu, P.V.R., Parihar, P.S. and Maithani, P.B. (2012) Geochemistry of Uraniferous Banganapalle Sediments in the Western Part of Palnad Sub-Basin, Andhra Pradesh: Implications on Provenance and Paleo-Weathering. Gondwana Geological Magasine. Special, 13, 1-14.
36. Jones, B. and Manning, D.C. (1994) Comparison of Geochemical Indices Used for the Interpretation of Paleo-Redox Conditions in Ancient Mudstones. Chemical Geology, 111, 110-131. https://doi.org/10.1016/0009-2541(94)90085-X
37. Olungbenga, A.O. and Olubunmi, I. (2012) The Geochemistry of Claystone-Shale Deposits from the Maastritchian Patti Formation, Southern Bida Basin, Nigeria. Earth Sciences Research Journal, 16, 3-8.
38. Nath, B.N., Bau, M., Ramalingeswara Rao, B. and Rao, Ch.M. (1997) Trace and Rare Earth Elemental Variation in Arabian Sea Sediments through a Transect across the Oxygen Minimum Zone. Geochimica et Cosmochimica Acta, 61, 2375-2388. https://doi.org/10.1016/S0016-7037(97)00094-X
39. Bowden, P., Van Breemen, O., Hutchison, J. and Turner, D.C. (1976) Palaeozoic and Mesozoic Age Trends for Some Ring Complexes in Niger and Nigeria. Nature, 259, 297299. https://doi.org/10.1038/259297a0
40. Roser, B.P. and Korsch, R.J. (1986) Determination of Tectonic Setting of Sandstone. Mudstone Suites Using SiO2 Content and K2O/Na2O Ratio. Journal of Geology, 94, 635-650. https://doi.org/10.1086/629071

41. Herron, M.M. (1988) Geochemical Classification of Terrigenous Sands and Shales from Core or Log Data. Journal of Sedimentary Research, 58, 820-829.
42. Roser, B.P. and Korsch, R.J. (1988) Provenance Signatures of Sandstone-Mudstone Suites Determined Using Discriminant Function Analysis of Major-Element Data. Chemical Geology, 67, 119-139. https://doi.org/10.1016/0009-2541(88)90010-1
43. Suttner, L.J. and Dutta, P.K. (1986) Alluvial Sandstones Composition and Paleoclimate, I, Framework Mineralogy. Journal of Sedimentary Petrology, 56, 329-345.
44. Armstrong-Altrin, J.S. and Verma, S.P. (2005) Critical Evaluation of Six Tectonic Setting Discrimination Diagrams Using Geochemical Data of Neogene Sediments from Known Tectonic Settings. Sedimentary Geology, 177, 115-129. https://doi.org/10.1016/j.sedgeo.2005.02.004
45. Bailey, J.C. (1981) Geochemical Criteria for a Refined Tectonic Discrimination of Orogenic Andesites. Chemical Geology, 38, 27-34. https://doi.org/10.1016/0009-2541(81)90135-2
46. Murphy (2000) In Book of Geochemistry of Sedimentary Rocks: Provenance, Paleoweathering and Tectonic Setting. 71-75.